Charge Density Waves and Electronic Properties of Superconducting Kagome Metals

Hengxin Tan, Yizhou Liu, Ziqiang Wang, and Binghai Yan

Charge density waves and electronic properties of superconducting kagome metals

Hengxin Tan,[1] Yizhou Liu,[1] Ziqiang Wang,[2] and Binghai Yan[1, *]

[1] *Department of Condensed Matter Physics, Weizmann Institute of Science, Rehovot 7610001, Israel*
[2] *Department of Physics, Boston College, Chestnut Hill, Massachusetts 02467, USA*
(Dated: June 24, 2021)

Kagome metals AV_3Sb_5 (A = K, Rb, and Cs) exhibit intriguing superconductivity below $0.9 \sim 2.5$ K, a charge density wave (CDW) transition around $80 \sim 100$ K, and $\mathbb{Z}_2$ topological surface states. The nature of the CDW phase and its relation to superconductivity remains elusive. In this work, we investigate the electronic and structural properties of CDW by first-principles calculations. We reveal an *inverse* Star of David deformation as the $2 \times 2 \times 2$ CDW ground state of the kagome lattice. The kagome lattice shows softening breathing-phonon modes, indicating the structural instability. However, electrons play an essential role in the CDW transition via Fermi surface nesting and van Hove singularity. The inverse Star of David structure agrees with recent experiments by scanning tunneling microscopy (STM). The CDW phase inherits the nontrivial $\mathbb{Z}_2$-type topological band structure. Further, we find that the electron-phonon coupling is too weak to account for the superconductivity T_c in all three materials. It implies the existence of unconventional pairing of these kagome metals. Our results provide essential knowledge toward understanding the superconductivity and topology in kagome metals.

The kagome lattice constitutes uniformly tiled triangles and hexagons in a plane. Related insulating materials are intensively studied for intriguing phenomena like spin liquid [1], geometrical frustration[2], charge density wave (CDW)[3], and unconventional superconductivity of doped Mott insulators[4]. For the more recent interest of topology, several magnetic kagome metals were found to be magnetic Weyl semimetals[5–7] and exhibit a large anomalous Hall effect[8–11]. Very recently, nonmagnetic kagome metals AV_3Sb_5 (A = K, Rb, and Cs)[12] were reported to exhibit both CDW and superconductivity, and $\mathbb{Z}_2$-type nontrivial band topology[13, 14], which sparked immediate interest in these materials[15–18].

The AV_3Sb_5 compounds exhibit a uniform kagome lattice of V atoms at room temperature. Calculations and angle-resolved photoemission spectroscopy[13] found the $\mathbb{Z}_2$ type topology in their band structure. These materials go through a CDW transition as cooling down to about $80 \sim 100$ K. From the CDW phases, they exhibit superconductivity with $T_c = 0.9 \sim 2.5$ K (see Table I for a summary). In CsV_3Sb_5, very recent experiments reveal possible nodal superconductivity [19] and the competition between superconductivity and CDW[20]. For the CDW phase, X-ray diffraction[13, 14] and scanning tunneling microscopy (STM)[21–24] revealed the formation of a 2×2 superlattice, for which Ref. 21 assumed a Star of David (SD) distortion in the kagome plane and the proximity of the Fermi surface to the van Hove singularity. However, solid knowledge of the lattice and electronic properties for the CDW state is missing to understand the superconductivity and topology.

In this work, we have investigated the structural and electronic properties of the CDW phase by first-principles density-functional theory [25] calculations. We find that
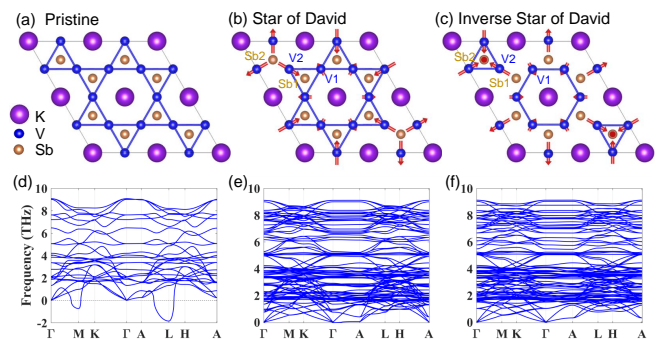
* binghai.yan@weizmann.ac.il

Figure 1. Crystal structures of KV_3Sb_5 in the pristine phase, the Star of David 2×2 CDW phase, and the inverse Star of David phase. Corresponding phonon dispersions are shown in the lower panels. A 2×2 supercell is shown in (a). Imaginary (negative) phonon frequency in (d) corresponds to the breathing mode of the kagome lattice. Such a breathing-instability is related to CDW distortions. The breathing-out and breathing-in lead to two different structures in (b) and (c), where the red arrows indicate the lattice distortion due to the breathing mode. In CDW phases, V1 and V2 represent inequivalent vanadium sites of the kagome lattice, and Sb1 and Sb2 are inequivalent sites of the honeycomb lattice.

the CDW transition is related to breathing phonon modes of the kagome lattice and electronically mediated by the Fermi surface instability. The resultant 2×2 CDW favors an *inverse* Star of David (ISD) deformation rather than the SD energetically for all three compounds. The STM images simulated for the ISD phase agree with the recent experiment. The CDW distortion modulates the Fermi surface but preserves the $\mathbb{Z}_2$ topology of the pristine phase. We find the electron-phonon coupling too weak to interpret the superconductivity for three materials. It may indicate the existence of unconventional superconductivity pairing.

CDW deformation – The pristine phase of AV_3Sb_5 crystallizes in the hexagonal structure with the space group of
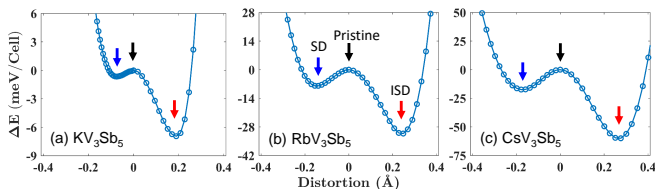
Figure 2. Total energy profiles for the three compounds. The distortion stands for the amplitude of the breathing phonon mode where the negative values are used for Star of David (SD) in order to distinguish from inverse Star of David (ISD). The ΔE stands for the relative total energy with respect to the pristine phase per supercell (36 atoms). Spin-orbit coupling is considered.
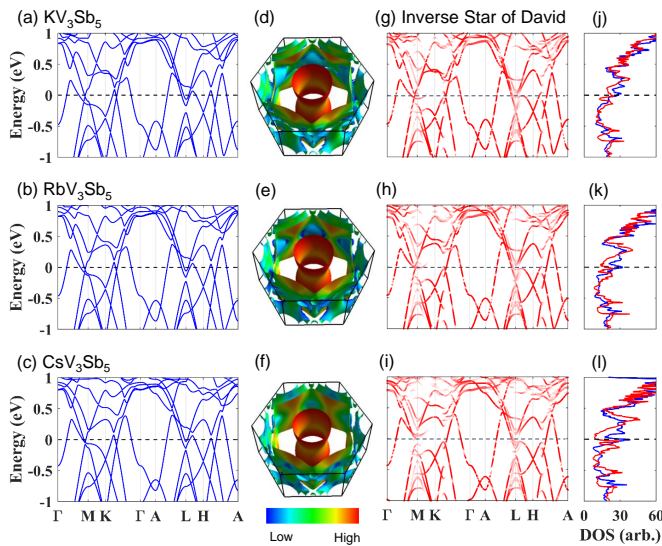

Figure 3. Electronic structures. (a-c) show the band structure for the pristine phase. (d-f) show the Fermi surface for the pristine phase, where the color stands for the Fermi velocity. (g-i) show the unfolded band structure of the inverse Star of David phase where the color represents the 1×1 spectrum weights. (j-l) show the total DOS of the pristine (blue) and inverse Star of David (red) phases. Spin-orbit coupling is included.

$P6/mmm$ (No.191), as shown in Fig. 1(a). The V atoms form the kagome layer, with Sb occupying V hexagon centers. Two additional honeycomb layers of Sb atoms sandwich the kagome lattice. Three materials are non-magnetic in our calculations, consistent with experiments [12, 26].

The pristine phases exhibit structural instability. We take KV$_3$Sb$_5$ as an example. Its phonon band structure in Fig. 1(d) shows softening acoustic phonon modes at the Brillouin zone boundary near M and L points, indicating the strong instability. Extended to the 2×2 supercell, the M-point soft mode corresponds to a breathing phonon (A_{1g} symmetry) of V atoms in the kagome lattice [Figs. 1(b) and (c)]. Breathing-in and out lead to two different structures. The SD structure forms when V1 (V2) atoms

move away (toward) the center, which is similar to the known CDW in 1T TaS$_2$[27]. The ISD structure forms by an inverse deformation to the SD. Both SD and ISD exhibit an in-plane 2×2 modulation of the structure. The superlattice shares the same space group of $P6/mmm$ as the pristine phase but has two inequivalent sites (i.e., V1 and V2 in Figs. 1) in the kagome plane. In addition, the L-point soft mode [Fig.1(d)] indicates the existence of a $2 \times 2 \times 2$ reconstruction. We will first investigate the 2×2 CDW and then discuss the inter-layer stacking pattern.

The optimized SD and ISD structures are locally stable for all three compounds, where the breathing deformation reduces the total energy. The imaginary frequencies disappear in their phonon spectra except for a faint soft feature in the SD case (see more details in the Supplementary Material (SM)[25]). It should be noted that structure optimizations are independent from phonon calculations. We find that the SD phase is higher in energy than the ISD phase for all three materials. As shown in Fig. 2, from K, to Rb and Cs, the ISD phase is more energetically favored, and the lattice displacement also becomes larger and larger. Therefore, the ISD phase is more likely the ground state structure than SD in the 2×2 CDW. In addition, the calculated diffraction pattern of ISD agrees better with experiments[13] than that of SD[25]. The ISD phase will be verified further by simulated STM images in the following.

The CDW is induced by the Peierls instability related to the Fermi surface nesting and phonon softening[28, 29]. The q vector of the soft phonon at M coincides with the Fermi nesting vector between neighboring van Hove singularities in the Fermi surface of AV$_3$Sb$_5$ (see Fig.3). Consequently, the CDW deformation strongly decreases the density of states (DOS) at the Fermi energy by suppressing the van Hove singularities. Related Fermi surface nesting, CDW, and their competition with superconductivity are extensively discussed for the kagome lattice model in literature[30–33]. Additionally, the phonon-softening at M and L can be suppressed if we artificially increase the *electron* temperature in DFT calculations [25]. Therefore, the electronic instability may play an essential role to drive the CDW transition, compared to phonons.

Above energetics and structures of two CDW phases are studied for bulk materials. When forming a surface with different charging or atomic-terminations, the ISD or SD structure may deviate on the surface. To examine the CDW stability on the surface, we have performed surface calculations using a slab model. Recent experiments[21, 22, 24] observed both A and Sb terminations on cleavage surfaces. We find that the ISD phase is still as stable as the bulk phase for the A-termination. However, the ISD deformation becomes weaker (closer to the pristine case) on the Sb-terminated surface than in the bulk. The SD phase exhibits a similar trend. Nevertheless, the ISD structure is still more energetically favored than the SD one. The surface atomic relaxation indicates the instability of the 2×2 CDW on the Sb-terminated surface. We note that recent STMs[22, 24] observed a 4×1 pattern
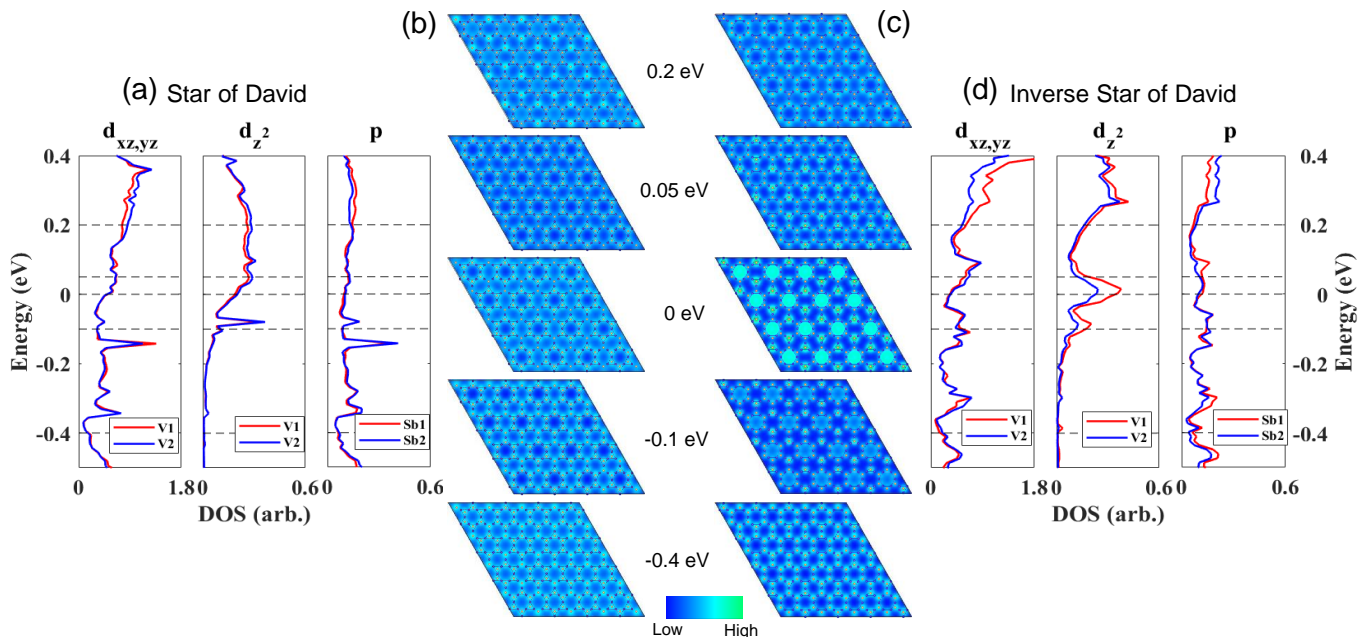
(a) Star of David

$d_{xz,yz}$ d_{z^2} p

Energy (eV)

0.4 0.2 0 -0.2 -0.4

V1 V2   V1 V2   Sb1 Sb2

0   1.80   0.60   0.6

DOS (arb.)

(b)

0.2 eV

0.05 eV

0 eV

-0.1 eV

-0.4 eV

(c)

Low   High

(d) Inverse Star of David

$d_{xz,yz}$ d_{z^2} p

0.4 0.2 0 -0.2 -0.4

Energy (eV)

V1 V2   V1 V2   Sb1 Sb2

0   1.80   0.60   0.6

DOS (arb.)

Figure 4. Surface orbital-resolved DOS and simulated STM images for the 2×2 CDW phases of KV$_3$Sb$_5$: (a) and (b) for the Star of David structure, (c) and (d) for the inverse Star of David structure. The DOS of V-d and Sb-p states are projected. The V1, V2, Sb1 and Sb2 in (a) and (d) are labeled in Fig. 1 (b) and (c) and superposed on the images for reference.

when the samples are cooled down further after the 2×2 CDW transition. The emerging 4×1 pattern may be due to electron correlations related to above surface instability and electron-phonon interaction.

Further, the very recent STM measurement[23] revealed a three-dimensional CDW, i.e., the $2 \times 2 \times 2$ CDW, for CsV$_3$Sb$_5$. This coincides with the inter-layer instability characterized by the soft phonon mode at the L (0.5, 0.5, 0.5) point in the phonon spectrum [Fig.1(d)]. Our calculations confirm that the π CDW-phase-shift between neighboring layers reduces slightly the binding energy by ~ 10 meV per 2×2 layer for CsV$_3$Sb$_5$ [25]. In the $2 \times 2 \times 2$ CDW, the SD phase is no longer meta-stable and relaxes to the ISD structure spontaneously. Therefore, the ISD deformation is still preferred. We note that the K and Rb compounds exhibit similar 3D CDW to the Cs one in calculations. Additionally, the $2 \times 2 \times 2$ CDW exhibits similar electronic structure as the $2 \times 2 \times 1$ one, because of the weak inter-layer interaction. For simplicity of analysis, we focus on the $2 \times 2 \times 1$ (i.e., 2×2) CDW phase in the following discussions.

Band structure and Fermi surface – The band structures of the pristine phase are shown in Fig. 3(a)-(c) for three materials, which are similar to the previous report. We should note that the Fermi energy (charge neutral point) in our work is about 0.1 eV higher than that of Ref.[12]. Such a minor derivation lifts the Fermi energy above the van Hove singularity point at M and leads to a slightly different Fermi surface (FS) near the Brillouin zone boundary [Fig. 3(d)-(f)]. The FSs exhibit a strong 2D feature and include the cylinder-like FS (Sb-p_z

states) centered around Γ, and the large hexagonal FS (V-d states). There are also much smaller FSs (V-d states) near M/L and K/H. Additionally, one can also observe the 2D feature in the weak $\Gamma - A$ dispersion in the phonon spectrum [Fig.1(d)].

The 2×2 ISD CDW distortion modifies the FSs. We unfold the band structure of the ISD phase to the pristine Brillouin Zone in Figs. 3(g)-(i). These bands near the Brillouin Zone boundary (e.g., M and K) are strongly modified, including the large hexagonal FS and small FSs. It is not surprising that the breathing distortion changes mainly the V-d driven states and especially suppresses the van Hove singularities slightly below the Fermi energy at M. Consequently, CDW reduces the total density of states (DOS) near the Fermi energy [Fig. 3(j)-(l)], which is also consistent with recent STM spectra[21, 24]. The Cs compound exhibits stronger FS and DOS modifications than the K and Rb compounds, because the lattice distortion is the largest for Cs (see Fig.2).

Different from V-d driven FSs, the cylinder-like FS from Sb-p_z is marginally affected by the CDW deformation, as shown in Fig.3. Because the breathing distortion mainly involves the V-kagome lattice, the CDW and electron-lattice interaction[25] are band-selective. This rationalizes the STM quasiparticle interference patterns in Refs. 22 and 23, where the Sb-p_z band around Γ is not affected by the CDW (either 2×2 or 4×1).

The band structure of the pristine phase displays non-trivial band inversion[13, 14]. For the CDW phases, we calculate the $\mathbb{Z}_2$ topological invariants[34] and find that both SD and ISD phases are still nontrivial topological

metals (see Ref.[25] for details).

Simulated STM images – STM images can examine the electronic and lattice structures of SD/ISD CDW in experiments. Therefore, we have simulated STM images for two CDW phases for all three materials. We also take the K compound as an example here since the Rb and Cs compounds share similar features[25]. We have calculated the local density of states (LDOS) in the plane that is ~ 3 Å above the Sb-terminated surface (in a slab model[25]) to simulate the STM dI/dV mapping. For a given bias V_b, the LDOS is summed in the energy range of $V_b \pm 25$ meV. Figures 4(a)&(d) show the surface DOS contributed by V1, V2, Sb1 and Sb2 atoms [labeled in Fig. 1(b) and (c)], to rationalize the bias dependence of STM images.

The most characteristic feature near the Fermi energy is that the ISD structure exhibits large, bright 2×2 spots by the V1-hexagon centers. In contrast, the SD structure exhibits bright circles around the V1-hexagon, with the hexagon center being dark. For ISD, the V1-hexagon centers turn quickly dark as moving away from the zero energy, which agrees with the recent STM for KV$_3$Sb$_5$ in Ref.[21]. Also supported by the lower total energy, we conclude that the ground state of the 2×2 CDW phase corresponds to the ISD structure for these three compounds. The high LDOS at V1-hexagon centers is caused by the large peak of V1-d_{z^2} and small V1-$d_{xz,yz}$ in DOS [Fig.4(d)]. In contrast, no such a V1-d_{z^2} peak appears for the SD surface [Fig.4(a)].

At $V_b = 0.05$ eV, the V1-hexagon brightness dramatically decreases due to the decreasing DOS of V-d_{z^2} on the ISD surface. At the same time, the V-$d_{xz,yz}$ DOS increases, where the V2-$d_{xz,yz}$ contribution is slightly larger than the V1-$d_{xz,yz}$ one. Thus, small V2-triangles turn brighter. For the SD surface, the STM image at $V_b = 0.05$ eV remains almost the same as that at zero because the relative amplitudes of DOS between V1 and V2 are nearly unchanged. For $V_b = 0.2$ eV, the ISD surface exhibits bright circles because V1 is larger in DOS than V2. In contrast, the SD surface shows small, bright spots at V2-triangles, caused by the relatively larger DOS of V2 than that of V1.

At $V_b = -0.1$ eV, the ISD surface looks less-contrast in the STM image than the zero bias case due to the decreasing V-d_{z^2} and increasing V-$d_{xz,yz}$ in DOS. For the SD surface, all the atomic sites show similar brightness due to the small DOS peaks of V-d and Sb-p near -0.1 eV. At $V_b = -0.4$ eV, both ISD and SD surfaces show a 1×1 honeycomb pattern. The honeycomb feature reflects the top Sb layer (Sb1 and Sb2), despite that V is comparable to Sb in DOS.

Superconductivity – AV$_3$Sb$_5$ exhibits superconductivity from the CDW normal state. The most recent STM on CsV$_3$Sb$_5$ reveals a superconducting gap $\Delta \sim 0.5$ meV[24], which puts the superconductor in the strong-coupling regime with $2\Delta/k_B T_c \sim 5$. A natural question is whether the superconductivity is driven by the electron-phonon coupling in Bardeen-Cooper-Schrieffer (BCS) scenario [35]. Therefore, we have calculated the electron-phonon

Table I. Estimation of the T_c due to electron-phonon coupling. We list the CDW transition temperature $T_{\mathrm{CDW}}^{\mathrm{exp.}}$, experimental superconducting temperature $T_c^{\mathrm{exp.}}$ and experimental Debye temperature $\theta_D^{\mathrm{exp.}}$ in unit of K [13–15]. Parameters and results: DOS N_F per superlattice at the Fermi energy (eV^{-1}), deformation potential D (eV/Å), phonon mediated electron-electron attractive interaction strength λ, calculated Debye temperature θ_D, and calculated T_c for the ISD phase. We choose the screened-repulsive interaction (μ^*) as 0.12 [36, 37]. More details are in SM [25].

	$T_{\mathrm{CDW}}^{\mathrm{exp.}}$	N_F	D	λ	θ_D	$\theta_D^{\mathrm{exp.}}$	T_c	$T_c^{\mathrm{exp.}}$
KV$_3$Sb$_5$	78	11.6	0.47	0.38	154	141	0.22	0.93
RbV$_3$Sb$_5$	102	9.3	0.50	0.32	176	169	0.05	0.92
CsV$_3$Sb$_5$	94	5.2	0.69	0.25	142	–	0.0008	2.5

coupling for the ISD phase and estimated the T_c based on McMillan's formula. Table I lists the calculated T_c for ISD phases of three materials. The deformation potentials (D) are one order of magnitude smaller than the known BCS superconductor MgB$_2$ [36]. The phonon-mediated attractive interaction(λ) is smaller than 1, indicating that three materials are in the weakly-coupled regime. It is in contradiction with the experimental indication from the superconducting gap mentioned above. The smallness of λ for CsV$_3$Sb$_5$ is mainly due to the low DOS (N_F) at the Fermi energy. The calculated T_c values are much smaller than the corresponding experimental values. Especially, phonons alone cannot account for the experimentally determined strong coupling superconductivity in CsV$_3$Sb$_5$. It indicates the unconventional mechanism of the superconductivity observed in these materials. In addition, we expect that the DOS reduction at the Fermi energy due to the CDW will lead to a Tc reduction. In this sense, the CDW and superconductivity are competing which is an interesting question for future study.

In summary, we have studied the lattice and electronic structures of the CDW phases of three kagome metals AV$_3$Sb$_5$. The 2×2 CDW (also the $2 \times 2 \times 2$ one) phase exhibits an inverse Star of David deformation. Corresponding STM images simulated agree with recent experiments. The nontrivial $\mathbb{Z}_2$ nature remains in the CDW band structure. We have evaluated the superconducting temperatures induced by electron-phonon coupling and found they are much smaller than experimental values, implying possible unconventional superconductivity in these materials.

[1] Matthew P Shores, Emily A Nytko, Bart M Bartlett, and Daniel G Nocera, "A structurally perfect s= 1/2 kagome antiferromagnet," Journal of the american chemical society **127**, 13462–13463 (2005).

[2] A P Ramirez, "Strongly geometrically frustrated magnets," Annual Review of Materials Science **24**, 453–480 (1994).

[3] S. V. Isakov, S. Wessel, R. G. Melko, K. Sengupta, and Yong Baek Kim, "Hard-Core Bosons on the Kagome Lattice: Valence-Bond Solids and Their Quantum Melting," Physical Review Letters **97**, 147202 (2006).

[4] Wing-Ho Ko, Patrick A. Lee, and Xiao-Gang Wen, "Doped kagome system as exotic superconductor," Physical Review B **79**, 214502 (2009).

[5] Hao Yang, Yan Sun, Yang Zhang, Wu-Jun Shi, Stuart S P Parkin, and Binghai Yan, "Topological Weyl semimetals in the chiral antiferromagnetic materials Mn3Ge and Mn3Sn," New Journal of Physics **19**, 015008 (2017).

[6] Noam Morali, Rajib Batabyal, Pranab Kumar Nag, Enke Liu, Qiunan Xu, Yan Sun, Binghai Yan, Claudia Felser, Nurit Avraham, and Haim Beidenkopf, "Fermi-arc diversity on surface terminations of the magnetic weyl semimetal co3sn2s2," Science **365**, 1286–1291 (2019).

[7] DF Liu, AJ Liang, EK Liu, QN Xu, YW Li, C Chen, D Pei, WJ Shi, SK Mo, P Dudin, *et al.*, "Magnetic weyl semimetal phase in a kagomé crystal," Science **365**, 1282–1285 (2019).

[8] Satoru Nakatsuji, Naoki Kiyohara, and Tomoya Higo, "Large anomalous Hall effect in a non-collinear antiferromagnet at room temperature," Nature **527**, 212 – 215 (2015).

[9] A K Nayak, J E Fischer, Y. Sun, B Yan, J Karel, A C Komarek, C Shekhar, N Kumar, W Schnelle, J Ku bler, C. Felser, and S.S.P. Parkin, "Large anomalous Hall effect driven by a nonvanishing Berry curvature in the noncolinear antiferromagnet Mn3Ge," Science Advances **2**, e1501870 – e1501870 (2016).

[10] Enke Liu, Yan Sun, Nitesh Kumar, Lukas Muechler, Aili Sun, Lin Jiao, Shuo-Ying Yang, Defa Liu, Aiji Liang, Qiunan Xu, Johannes Kroder, Vicky Suess, Horst Borrmann, Chandra Shekhar, Zhaosheng Wang, Chuanying Xi, Wenhong Wang, Walter Schnelle, Steffen Wirth, Yulin Chen, Sebastian T B Goennenwein, and Claudia Felser, "Giant anomalous Hall effect in a ferromagnetic kagome-lattice semimetal," Nature Physics **14**, 1125 – 1131 (2018).

[11] Linda Ye, Mingu Kang, Junwei Liu, Felix Von Cube, Christina R Wicker, Takehito Suzuki, Chris Jozwiak, Aaron Bostwick, Eli Rotenberg, David C Bell, *et al.*, "Massive dirac fermions in a ferromagnetic kagome metal," Nature **555**, 638–642 (2018).

[12] Brenden R. Ortiz, Ldia C. Gomes, Jennifer R. Morey, Michal Winiarski, Mitchell Bordelon, John S. Mangum, Iain W. H. Oswald, Jose A. Rodriguez-Rivera, James R. Neilson, Stephen D. Wilson, Elif Ertekin, Tyrel M. McQueen, and Eric S. Toberer, "New kagome prototype materials: discovery of KV_3Sb_5, RbV_3Sb_5, and CsV_3Sb_5," Physical Review Materials **3**, 094407 (2019).

[13] Brenden R. Ortiz, Samuel M. L. Teicher, Yong Hu, Julia L. Zuo, Paul M. Sarte, Emily C. Schueller, A. M. Milinda Abeykoon, Matthew J. Krogstad, Stephan Rosenkranz, Raymond Osborn, Ram Seshadri, Leon Balents, Junfeng He, and Stephen D. Wilson, "CsV_3Sb_5: A Z_2 Topological Kagome Metal with a Superconducting Ground State," Physical Review Letters **125**, 247002 (2020).

[14] Brenden R. Ortiz, Paul M. Sarte, Eric M. Kenney, Michael J. Graf, Samuel M. L. Teicher, Ram Seshadri, and Stephen D. Wilson, "Superconductivity in the F_2 kagome metal kv_3sb_5," Phys. Rev. Materials **5**, 034801 (2021).

[15] Qiangwei Yin, Zhijun Tu, Chunsheng Gong, Yang Fu, Shaohua Yan, and Hechang Lei, "Superconductivity and normal-state properties of kagome metal rbv_3sb_5 single crystals," Chinese Physics Letters **38**, 037403 (2021).

[16] Shuo-Ying Yang, Yaojia Wang, Brenden R. Ortiz, Defa Liu, Jacob Gayles, Elena Derunova, Rafael Gonzalez-Hernandez, Libor mejkal, Yulin Chen, Stuart S. P. Parkin, Stephen D. Wilson, Eric S. Toberer, Tyrel McQueen, and Mazhar N. Ali, "Giant, unconventional anomalous Hall effect in the metallic frustrated magnet candidate, KV3Sb5," Science Advances **6**, eabb6003 (2020).

[17] F H Yu, T Wu, Z Y Wang, B Lei, W Z Zhuo, J J Ying, and X H Chen, "Concurrence of anomalous Hall effect and charge density wave in a superconducting topological kagome metal," arXiv:2102.10987 (2021).

[18] Yaojia Wang, Shuoying Yang, Pranava K Sivakumar, Brenden R Ortiz, Samuel M L Teicher, Heng Wu, Abhay K Srivastava, Chirag Garg, Defa Liu, Stuart S P Parkin, Eric S Toberer, Tyrel McQueen, Stephen D Wilson, and Mazhar N Ali, "Proximity-induced spin-triplet superconductivity and edge supercurrent in the topological Kagome metal, $K_{1-x}V_3Sb_5$," arXiv:2012.05898 (2020).

[19] C C Zhao, L S Wang, W Xia, Q W Yin, J M Ni, Y Y Huang, C P Tu, Z C Tao, Z J Tu, C S Gong, H C Lei, Y F Guo, X F Yang, and S Y Li, "Nodal superconductivity and superconducting dome in the topological Kagome metal CsV3Sb5," arXiv:2102.08356 (2021).

[20] K Y Chen, N N Wang, Q W Yin, Z J Tu, C S Gong, J P Sun, H C Lei, Y Uwatoko, and J G Cheng, "Double superconducting dome and triple enhancement of Tc in the kagome superconductor CsV3Sb5 under high pressure," arXiv:2102.09328 (2021).

[21] Yu-Xiao Jiang, Jia-Xin Yin, M Michael Denner, Nana Shumiya, Brenden R Ortiz, Junyi He, Xiaoxiong Liu, Songtian S Zhang, Guoqing Chang, Ilya Belopolski, Qi Zhang, Md Shafayat Hossain, Tyler A Cochran, Daniel Multer, Maksim Litskevich, Zi-Jia Cheng, Xian P Yang, Zurab Guguchia, Gang Xu, Ziqiang Wang, Titus Neupert, Stephen D Wilson, and M Zahid Hasan, "Discovery of topological charge order in kagome superconductor KV_3Sb_5," arXiv:2012.15709 (2020).

[22] He Zhao, Hong Li, Brenden R Ortiz, Samuel M L Teicher, Taka Park, Mengxing Ye, Ziqiang Wang, Leon Balents, Stephen D Wilson, and Ilija Zeljkovic, "Cascade of correlated electron states in a kagome superconductor CsV3Sb5," arXiv:2103.03118 (2021).

[23] Zuowei Liang, Xingyuan Hou, Wanru Ma, Fan Zhang,

Ping Wu, Zongyuan Zhang, Fanghang Yu, J. J. Ying, Kun Jiang, Lei Shan, Zhenyu Wang, and X. H. Chen, "Three-dimensional charge density wave and robust zero-bias conductance peak inside the superconducting vortex core of a kagome superconductor CsV3Sb5," arXiv:2103.04760 (2021).

[24] Hui Chen, Haitao Yang, Bin Hu, Zhen Zhao, Jie Yuan, Yuqing Xing, Guojian Qian, Zihao Huang, Geng Li, Yuhan Ye, Qiangwei Yin, Chunsheng Gong, Zhijun Tu, Hechang Lei, Shen Ma, Hua Zhang, Shunli Ni, Hengxin Tan, Chengmin Shen, Xiaoli Dong, Binghai Yan, Ziqiang Wang, and Hong-Jun Gao, "Roton pair density wave and unconventional strong-coupling superconductivity in a topological kagome metal," arXiv:2103.09188 (2021).

[25] See Supplemental Material for more information about the method, crystal structures, electronic structures, phonon properties and STM images, which includes Refs. [38–47].

[26] Eric M Kenney, Brenden R Ortiz, Chennan Wang, Stephen D Wilson, and Michael Graf, "Absence of local moments in the kagome metal KV_3Sb_5 as determined by muon spin spectroscopy," Journal of Physics: Condensed Matter 33, 235801 (2021).

[27] J.A. Wilson, F.J. Di Salvo, and S. Mahajan, "Charge-density waves and superlattices in the metallic layered transition metal dichalcogenides," Advances in Physics 24, 117–201 (1975).

[28] Rudolf Ernst Peierls, *Quantum theory of solids* (Clarendon Press, 1996).

[29] W. Kohn, "Image of the fermi surface in the vibration spectrum of a metal," Phys. Rev. Lett. 2, 393–394 (1959).

[30] Jun Wen, Andreas Rüegg, C. C. Joseph Wang, and Gregory A. Fiete, "Interaction-driven topological insulators on the kagome and the decorated honeycomb lattices," Phys. Rev. B 82, 075125 (2010).

[31] Shun-Li Yu and Jian-Xin Li, "Chiral superconducting phase and chiral spin-density-wave phase in a Hubbard model on the kagome lattice," Physical Review B 85, 144402 (2012).

[32] Maximilian L. Kiesel, Christian Platt, and Ronny Thomale, "Unconventional fermi surface instabilities in the kagome hubbard model," Phys. Rev. Lett. 110, 126405 (2013).

[33] Wan-Sheng Wang, Zheng-Zhao Li, Yuan-Yuan Xiang, and Qiang-Hua Wang, "Competing electronic orders on kagome lattices at van hove filling," Phys. Rev. B 87, 115135 (2013).

[34] Liang Fu and C. L. Kane, "Topological insulators with inversion symmetry," Phys. Rev. B 76, 045302 (2007).

[35] J. Bardeen, L. N. Cooper, and J. R. Schrieffer, "Theory of Superconductivity," Phys. Rev. 108, 1175–1204 (1957).

[36] J. M. An and W. E. Pickett, "Superconductivity of MgB_2: Covalent Bonds Driven Metallic," Phys. Rev. Lett. 86, 4366–4369 (2001).

[37] Chen Si, Zheng Liu, Wenhui Duan, and Feng Liu, "First-principles calculations on the effect of doping and biaxial tensile strain on electron-phonon coupling in graphene," Phys. Rev. Lett. 111, 196802 (2013).

[38] John P. Perdew, Kieron Burke, and Matthias Ernzerhof, "Generalized gradient approximation made simple," Phys. Rev. Lett. 77, 3865 (1996).

[39] Georg Kresse and Jürgen Furthmüller, "Efficiency of ab-initio total energy calculations for metals and semiconductors using a plane-wave basis set," Comput. Mater. Sci. 6, 15–50 (1996).

[40] G. Kresse and J. Furthmüller, "Efficient iterative schemes for ab initio total-energy calculations using a plane-wave basis set," Phys. Rev. B 54, 11169 (1996).

[41] P. E. Blöchl, "Projector augmented-wave method," Phys. Rev. B 50, 17953 (1994).

[42] Stefan Grimme, Jens Antony, Stephan Ehrlich, and Helge Krieg, "A consistent and accurate ab initio parametrization of density functional dispersion correction (DFT-D) for the 94 elements H-Pu," J. Chem. Phys. 132, 154104 (2010).

[43] Atsushi Togo and Isao Tanaka, "First principles phonon calculations in materials science," Scr. Mater. 108, 1–5 (2015).

[44] F. S. Khan and P. B. Allen, "Deformation potentials and electron-phonon scattering: Two new theorems," Phys. Rev. B 29, 3341–3349 (1984).

[45] W. L. McMillan, "Transition Temperature of Strong-Coupled Superconductors," Phys. Rev. 167, 331–344 (1968).

[46] Charles K Poole, Horacio A Farach, and Richard J Creswick, "Handbook of superconductivity," (Elsevier, 1999).

[47] MG Vergniory, L Elcoro, Claudia Felser, Nicolas Regnault, B Andrei Bernevig, and Zhijun Wang, "A complete catalogue of high-quality topological materials," Nature 566, 480–485 (2019).